HHS Public Access

Author manuscript

Colloids Surf B Biointerfaces. Author manuscript; available in PMC 2021 January 13.

Published in final edited form as:

Colloids Surf B Biointerfaces. 2019 June 01; 178: 44–55. doi:10.1016/j.colsurfb.2019.02.037.

Square prism micropillars on poly(methyl methacrylate) surfaces modulate the morphology and differentiation of human dental pulp mesenchymal stem cells

Onur Hasturk[a,b,1], **Menekse Ermis**[a,c], **Utkan Demirci**[d,e], **Nesrin Hasirci**[a,b,c,f], **Vasif Hasirci**[a,b,c,g,2,*]

[a]Middle East Technical University (METU) BIOMATEN Center of Excellence in Biomaterials and Tissue Engineering, Ankara 06800, Turkey

[b]METU, Graduate Department of Biotechnology, Ankara 06800, Turkey

[c]METU, Graduate Department of Biomedical Engineering, Ankara 06800, Turkey

[d]Bio-Acoustic-MEMs in Medicine (BAMM) Laboratory, Canary Center at Stanford for Cancer Early Detection, Department of Radiology, Stanford School of Medicine, Palo Alto, CA 94394, USA

[e]Electrical Engineering Department (by courtesy), Stanford University, Stanford, USA

[f]METU, Department of Chemistry, Ankara 06800, Turkey

[g]METU, Department of Biological Sciences, Ankara 06800, Turkey

Abstract

Use of soluble factors is the most common strategy to induce osteogenic differentiation of mesenchymal stem cells (MSCs) *in vitro,* but it may raise potential side effects *in vivo*. The topographies of the substrate surfaces affect cell behavior, and this could be a promising approach to guide stem cell differentiation. Micropillars have been reported to modulate cellular and subcellular shape, and it is particularly interesting to investigate whether these changes in cell morphology can modulate gene expression and lineage commitment without chemical induction. In this study, poly(methyl methacrylate) (PMMA) films were decorated with square prism micropillars with different lateral dimensions (4, 8 and 16 μm), and the surface wettability of the substrates was altered by oxygen plasma treatment. Both pattern dimensions and hydrophilicity were found to affect the attachment, proliferation, and most importantly, gene expression of human dental pulp mesenchymal stem cells (DPSCs). Decreasing the pillar width and interpillar

*Corresponding author. vhasirci@metu.edu.tr (V. Hasirci).

[1]Present address: Tufts University, Department of Biomedical Engineering, Medford, MA 02155, USA

[2]Present address: Acibadem Mehmet Ali Aydinlar University, Department of Medical Engineering, Atasehir, Istanbul 34752, Turkey

Conflict of Interest

The authors O.H., M.E., N.H. and V.H. declare no competing financial interests. U.D. is a founder of and has an equity interest in: (i) DxNow Inc., a company that is developing microfluidic and imaging technologies for point-of-care diagnostic solutions, and (ii) Koek Biotech, a company that is developing microfluidic IVF technologies for clinical solutions. U.D.'s interests were viewed and managed in accordance with the conflict of interest policies.

spacing enhanced cell attachment, cell elongation, and nuclear deformation of nuclei, but reduced early proliferation rate. Surfaces with 4 or 8 μm wide pillars/gaps upregulated the expression of early bone-marker genes and mineralization over 28 days of culture. Exposure to oxygen plasma increased wettability and promoted cell attachment and proliferation but delayed osteogenesis. Our findings showed that surface topography and chemistry are very useful tools in controlling cell behavior on substrates and they can even help create better implants. The most important finding is that hydrophobic micropillars on polymeric substrate surfaces can be exploited in inducing osteogenic differentiation of MSCs without any differentiation supplements.

Graphical Abstract

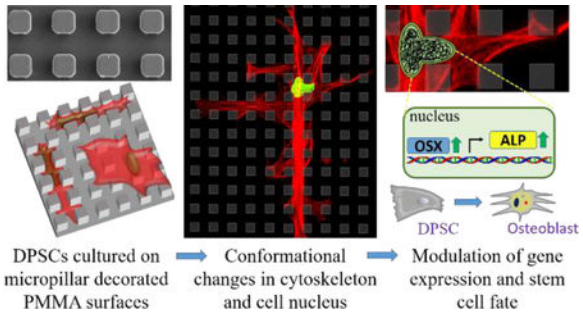

Keywords

Micropillars; dental pulp mesenchymal stem cells; cell morphology; proliferation; osteogenic differentiation

Introduction

Tissue engineering strategies have emerged as alternatives to auto- or allografts and implants in the regeneration of defected tissues in cases of massive bone losses or fractions[1–3]. MSCs have been of great interest in bone tissue engineering because of their high self-renewal and osteogenic capacity[4]. Human dental pulp has been identified as an easily accessible source of MSCs for clinical applications and dental pulp stem cells (DPSCs) have been shown to exhibit a high osteogenic/odontogenic capacity[5, 6]. Effective and safe induction of osteogenesis, however, has been an issue for the researchers. It is difficult to deliver soluble differentiation supplements such as bone morphogenetic proteins (BMPs) and dexamethasone in a spatially and temporally controlled manner to obtain satisfactory effects[7]. Moreover, their use raises safety concerns including the potential side effects and the risk of tumorigenicity in supraphysiological doses[8]. Besides biochemical factors, the fate of stem cells is also modulated by the topography of basement membranes, which regulate adhesion, distribution and organization of cytoskeletal elements, migration, survival, growth, and differentiation of adherent cells[9–11]. For example, changes in the morphology of BMSCs upon spreading on micro- and nanoscale topography of the collagen fibrils and hydroxyapatite crystals of the bone matrix contribute to their differentiation into osteoblasts[12, 13]. Then further differentiation into mechanosensitive osteocytes is triggered upon entrapment in bone lacunae of 10–30 μm diameters distorts the cuboid shape of

osteoblasts into a highly-branched morphology with numerous cytoplasmic extensions running along the narrow channels called canaliculi[14]. The mechanism by which these physical features modulate the cell fate has been explained with the mechanotransduction of local cytoskeletal tensions created by the changes in size and shape of the cells[11, 15]. These tensions or signals are transmitted from focal adhesion complexes to cell nucleus either indirectly, chemically, through the signaling cascades that modulate the activity of transcription factors[16], or directly through the linker proteins between the cytoskeletal filaments and nuclear lamina, resulting in a repositioning of chromatin and alteration of gene expression[17–20]. The modulation of cell morphology through surface topography may therefore be a safer alternative to soluble factors for guiding lineage commitment of stem cells.

The advances in lithographic micro- and nanostructure fabrication methods in silicon microelectronics industry have enabled researchers in biology and biomedicine to design surface structures to study the responses of cells to the surface topography[21, 22]. A variety of micro- and nanoscale 3D surface features including ridges and grooves, randomly or evenly distributed pits, pillars/posts, or wells[23, 24] have been shown to influence the attachment[25, 26], migration[27, 28], morphology[29, 30], proliferation[31–33], and differentiation of the cells[34–38]. Cells were reported to align themselves along the ridges of surface patterns through a phenomenon called contact guidance[39] and exhibit morphological changes in cell body[25, 40–44]. In addition to causing alterations of cell shape, micropillar-decorated surfaces with low micron sized cues were shown to trigger severe deformations in cell nuclei[33, 38, 45–50]. We also reported that DPSCs cultured on PMMA surfaces decorated with square prism micropillars displayed distinctive changes in cellular and nuclear shapes, the type and extent of which depended on the lateral dimensions and hydrophilicity of the pillars[51].

In a more recent study, we showed that micropillars improve osteogenic activity of human osteoblast-like cells on PMMA surfaces by promoting cell attachment, alkaline phosphatase (ALP) expression and mineralization[52]. Our findings address a fundamental question: besides improving osteogenic activity, could these micropillar decorated surfaces also induce osteogenic differentiation of mesenchymal stem cells without biochemical supplements? Changes in cellular[37, 53, 54] or nuclear[38] morphologies on patterned surfaces have been demonstrated to improve osteogenic differentiation of MSCs induced by differentiation media. Studies on the induction of stem cell differentiation on 3D topographical features without soluble factors, however, are limited. Examples of induction of osteogenesis by surface topography without chemical supplements include the culture of mesenchymal stem cells on artificial ECM[55], silk fibroin[56] and polyurethane[57] substrates but these substrates were decorated with submicron ridges and grooves, on PMMA surfaces decorated with randomly distributed nanopillars[34] and on tantalum coated microarrays with shallow (2.4 μm high) pillars[26]. In none of these studies, however, cytoskeletal and nuclear deformations were extensively induced, emphasized or correlated with osteogenesis.

Here we hypothesize that the osteogenic differentiation of DPSCs can be induced by micropillars through the modulation of cytoskeletal and nuclear morphologies and no differentiation supplements. We planned to assess the influence of induced morphological

changes on the fate of DPSCs by performing proliferation, osteogenic gene expression, bone matrix deposition and mineralization tests. For this purpose, a series of PMMA micropillar arrays with pillar widths and spacings in the size range of bone lacunae (4, 8 and 16 μm) were designed. The hydrophilicity of the substrates was improved by oxygen plasma treatment, which we had previously shown to induce morphological changes in a shorter time and to a higher extent[51]. Findings of this present study will lead to more defined topographical parameters for use in the design of tissue engineering scaffolds and bone implants with better osteoinduction and osseointegration capacities.

Materials and Methods

Fabrication and characterization of PMMA micropillar arrays

Poly(methyl methacrylate) (PMMA; $\overline{M}$w = 996kDa) was purchased from Sigma-Aldrich (USA). The production of silicon microarrays by typical photolithography, and the preparation of polymeric micropillar arrays by solvent casting on silicon array templates or wafers have been previously reported[45, 51, 52]. Three types of silicon wafers were decorated with 8 μm tall square prism pillars: P4G4, P8G8 and P16G16, where P is the lateral dimension of square prism pillars and G is the interpillar gap in μm. Poly(dimethyl siloxane) (PDMS) (Sylgard 184, Dow Corning Company, UK) negatives of the wafers were produced and PMMA replicates of the original wafers were fabricated by solvent casting of 20% (w/v) PMMA solution in chloroform (Avantor J.T. Baker, USA) on the PDMS molds. All films had a surface area of 0.64 cm^2. PMMA replicas were Au-Pd coated under vacuum and visualized using SEM (400 F Field Emission SEM, USA). Surface wettability of the substrates was improved by oxygen plasma treatment using a Femto 40 kHz Plasma System (Diener Electronic, Germany). The pressure in the plasma chamber was maintained at 20 mbar and the substrates were exposed to oxygen plasma at 100 W for 10 min. Samples were then immediately used in contact angle measurements and *in vitro* tests.

Cell isolation, culture and seeding protocol

Human dental pulp stem cells were isolated from a third molar teeth via an enzymatic degradation method as reported before[51, 58]. Human dental pulp extracts from impacted third molars were obtained from 3 patients (2 female, 1 male), aged 18–22 years, with informed written consent at the Middle East Technical University Medical Center with the approval of the METU Human Subjects Ethics Committee of, Ankara, Turkey (No: 28620816/505–69). Briefly, pulp tissue fragments were minced into small pieces and digested with collagenase type I and dispase II (Sigma-Aldrich, USA). Cells from 3 patients were filtered, pooled and expanded in DMEM:F12 1:1 (Lonza, Switzerland) supplemented with fetal bovine serum (FBS, 10%, v/v) (Biowest, France), penicillin and streptomycin (Pen-Strep, 100 $U.mL^{-1}$) and L-glutamine (5 mM) (Lonza, Switzerland). Passages 2–5 were used in the *in vitro* studies. Cells in the chemical induction group (control) were cultured on TCPS (n=3) in an expansion media supplemented with 100 nM dexamethasone, 10 mM β-glycerophosphate and 50 μM L-ascorbic acid (Sigma-Aldrich, USA).

Cells were seeded onto the substrates as described previously[45, 51]. Briefly, PMMA films were sterilized by exposing both sides to UV for 15 min and placed into 12-well plates.

Cells were detached from the tissue culture flasks, counted using Nucleocounter (Chemometec, Denmark), and seeded onto the patterned surfaces at a density of 10^4 cells.cm^{-2}. The number of seeded cells were found to be too high for a morphology analysis of individual cells even at early time points. It was, however, too low for the determination of cell numbers on Day 1 by Alamar Blue assay or for the extraction of enough mRNA on Day 7 for gene expression analysis. Cell seeding density was, therefore, optimized as 3×10^3 cells.cm^{-2} for microscopy, 10^4 cells.cm^{-2} for proliferation and immunofluorescence, and 3×10^4 cells.cm^{-2} for cell attachment and gene expression analyses. After 2 h of seeding, 2 mL of expansion medium was gently added to each well. Plates were incubated at 37°C and 5% CO_2 incubator, and the medium was changed every 2 days.

Flow cytometry

Isolated cells were characterized for the MSC negative and positive surface antigens by flow cytometry (BD Accuri C6, USA). Trypsinized cells were washed with FACS buffer (1:1000 sodium azide (Sigma-Aldrich) and 1:100 BSA (Sigma-Aldrich) in PBS) and fixed in 4% paraformaldehyde (Sigma-Aldrich) solution for 15 min. Fixed cells were stained with mouse IgG1 anti-human monoclonal antibodies (Biolegend, USA) against CD31 (#303110), CD45 (#304017), CD90 (#328116) and CD105 (#323212) and 10^5 cells were counted per sample.

Cell attachment and proliferation

Numbers of cells on the substrates were determined using the Alamar Blue® cell viability assay (Thermo Fisher Scientific, USA) 16 h after seeding and on Days 3, 7, 14 and 21. Substrates were washed twice with PBS and incubated in 500 µL Alamar blue solution (10% in DMEM High Glucose colorless (Lonza) supplemented with 100 U.mL^{-1} Pen-Strep) for 2 h at 37°C and 5% CO_2. Absorbance was measured twice for each sample (n=3) at 570 nm (reduced) and 595 nm (oxidized) using a plate reader (Multiscan Spectrum, Thermo Scientific). Dye reduction (%) was calculated as described in the assay guide, and it was converted to cell numbers using a calibration curve (Fig. S1). The specific growth rate of the DPSCs during the exponential growth phase were calculated by using the cell numbers and the Equation 2 which was derived from Equation 1[59]:

$$N_t = N_0 e^{\mu t} \tag{1}$$

$$\mu = \ln\left(\frac{N_t}{N_0}\right)/t \tag{2}$$

where N_t is the cell numbers at a specific time point within the exponential growth phase, N_0 the initial cell numbers on Day 3, t the time (d) and μ the specific growth rate (d^{-1}).

Scanning electron microscopy (SEM) imaging

Samples were rinsed with PBS, fixed in 4% paraformaldehyde, washed with PIPES (piperazine-N,N'-bis(ethanesulfonic acid)) buffer (Sigma-Aldrich, USA) and incubated in 1% osmium tetroxide (OsO_4) (Polysciences, USA) in PIPES buffer at RT for 1 h. Then, the samples were washed again with PIPES buffer and dehydrated by incubating in a series of

50, 70 and 100% (v/v) ethanol solutions at RT for 5 min each. Samples were Au-Pd coated under vacuum and examined by SEM.

Confocal scanning laser microscopy (CSLM) imaging

Samples were washed with PBS and fixed by immersing the samples in 4% (w/v) paraformaldehyde solution for 15 min at RT. Cells were permeabilized with Triton X-100 (PanReac Applichem, Germany) solution (0.1%, v/v, in PBS) for 5 min at RT. After washing with PBS, samples were incubated in BSA blocking solution (1%, w/v, in PBS) at 37°C for 30 min. Samples were incubated in Alexa Fluor 488 conjugated phalloidin (Thermo Fisher Scientific, USA) solution (1:50 in 0.1% BSA) at 37°C for 1 h and in DRAQ5 (ab108410, Abcam, UK) solution (1:1000 in 0.1% BSA) at RT for 1 h to label actin cytoskeleton and nuclei, respectively. Then, the samples were washed twice with PBS and analyzed by using Leica SPE confocal laser scanning microscope (Germany).

qRT-PCR

The total RNA was collected from 12-well culture plates (n=4) for the chemical induction group or n=4 samples (each repeat consisted of a pool of 5 separate PMMA replicas) on Days 7, 14, and 28 using Masterpure RNA Purification Kit (Epicentre, USA) according to the manufacturer's instructions. First-strand cDNAs were reverse transcribed using RevertAid First Strand cDNA Synthesis Kit (Thermo Fisher Scientific) from each sample using a thermal cycler (iCycler, BIORAD, USA). qRT-PCR reactions were performed using GoTaq® qPCR Mastermix (Promega, USA) with Rotor-Gene Q real-time PCR cycler (Qiagen, Germany) using forward and reverse primers specific for glyceraldehyde 3-phosphate dehydrogenase (GAPDH), Osterix (OSX), alkaline phosphatase (ALP) and osteocalcin (OC) listed in Supplementary Table 1. PCR conditions were: an initial denaturation at 95°C (2 min) and 35 cycles of denaturation at 95°C (15 s), and annealing/extension at 60°C (60 s). The C_t values for OSX, ALP and OC were normalized to that of the housekeeping gene GAPDH. Relative expression of the genes was calculated by the $\Delta\Delta C_t$ method as described elsewhere[60]. Briefly, the fold changes in gene expression ($2^{-\Delta\Delta Ct}$) by chemically induced cells on TCPS and by the cells cultured on micropatterned surfaces were calculated by normalization to expression levels in growth medium without osteogenic supplements and to expression levels on unpatterned control surfaces, respectively.

Immunofluorescence

Cells attached on the samples were fixed with paraformaldehyde solution. They were then incubated at 37°C for 1 h in blocking solution (5% v/v goat serum, 1% v/v Tween 20, 0.1% w/v BSA, 0.1% w/v sodium azide in 0.01 M PBS). For the immunostaining of collagen type I and osteopontin, samples were incubated within primary antibody (Rabbit anti-osteopontin, ab91655; mouse anti-collagen type I, ab23446, Abca, UK) for 1 h and in secondary antibody (Goat anti-Rabbit IgG Alexa Fluor 488, A-11008; Goat anti-Mouse IgG Alexa Fluor 532, A-11002, Invitrogen, USA) for 30 min. Cell nuclei were stained with DRAQ5 for 15 min at RT. After preparation, specimens were kept in the dark, humidified containers until microscopic examination. CLSM images were collected using Leica SPE

and the laser power was kept constant for each channel. Signal intensity for each marker was normalized to the signal intensity of nuclei to normalize matrix deposition to cell numbers.

Mineralization

Mineralization (calcium deposition) to evaluate the degree of osteogenesis on the samples was determined by Alizarin red staining. Samples were fixed in 4% paraformaldehyde solution for 15 min, rinsed with 0.01M PBS, stained with Alizarin Red S (Cyagen, USA) for 5 min and rinsed with 0.01M PBS before imaging. Images were collected with Olympus IX70 inverted light microscope (Japan) with a 20x objective.

Statistical Analysis

All quantitative data in this study ($n \geq 3$) are expressed as mean ± standard deviation. One-way analysis of variance (One-way ANOVA) with Tukey's pairwise comparison test was performed to analyze the results between the groups. p-values less than 0.05 were considered statistically significant. Pearson product moment correlation test was performed to calculate the correlation coefficients (r) between two variables. Variables with $|r|$ values larger than 0.5 and 0.85 were considered correlated and strongly correlated, respectively.

Results and Discussion

Characterization of micropillar decorated PMMA surfaces

The topographical features of the ECM are known to regulate the responses of MSCs. Therefore, engineering of substrate topography has been widely investigated in the last decade with the aim of guiding lineage commitment of stem cells[9, 23]. We prepared micropillar arrays on PMMA surfaces that we previously reported to generate distinct morphological changes in DPSCs[51]. Three types of PMMA surfaces with micropillars of 8 μm height and varying lateral dimensions (P4G4, P8G8 and P16G16 in Fig.1A, P and G represent the width of square pillars and interpillar gaps in μm, respectively) were prepared (Fig.1B). Unpatterned PMMA substrates were used as negative control surfaces. We previously showed that the Young's moduli (E: 1300 MPa) and ultimate tensile strength (UTS: 41 MPa) (Fig.S2) of solvent cast PMMA films were in the range of natural bone tissue (E: 100–30000 MPa, UTS: 5–150 MPa)[52], indicating that the mechanical properties of our substrates were suitable for osteogenesis. Wettability of polymeric surfaces modulates the type, amount, and conformation of the adsorbed proteins, which in turn influences adhesion, proliferation, and differentiation of mammalian cells[61]. O_2 plasma treatment introduces oxygen rich polar groups on substrate surfaces and modulate surface wettability, [62, 63], which is known to affect behavior of adherent cells[64]. A set of substrates were therefore exposed to oxygen plasma prior to cell seeding (Fig.1C) to investigate the influence of improved wettability of micropillar arrays and earlier and more robust alterations in cell morphology[51] on the fate of DPSCs. AFM analysis (Fig.S3) showed that oxygen plasma treatment slightly increased the nanoscale roughness of unpatterned surfaces, bringing RMS deviation from 6.4 to 15.9 nm and average height from 33.1 to 54.6 nm (Supplementary table 2).

Characterization of isolated cells

Cells isolated from dental pulps had MSC-like well spread, broad, and flattened shapes on TCPS (Fig.S4A) which is consistent with literature[58, 65]. Cells at passage 2 were found to be positive (>50%) for MSC surface markers CD90 (100%) and CD105 (73.6%) and negative for hematopoietic stem cell surface markers CD31 (0.3%) and CD45 (0.4%) (Fig.4A). The relatively lower expression of CD105 at low passages was consistent with other studies[66, 67], and it was increased significantly at passage 5 (99.6%, Fig.S4B) probably because of a gradual decrease in the proportion of CD105 negative ectomesenchymal stem cells that share a common origin with neural crest cells[67, 68].

DPSCs cultured on TCPS in osteogenic induction media displayed a significant increase in the expressions of OSX, ALP, and OC over 28 days of culture (Fig.2B), confirming the osteogenic capacity of the isolated cells. OSX expression was slightly upregulated on Day 7, followed by a 10-fold increase on Day 14, and a sharp decrease back to the baseline on Day 28. A similar observation was reported by Igarashi et al., who observed an initial increase of OSX expression with differentiating calvarial cells for the first 15 days and a gradual decrease afterwards[69]. Peak OSX levels on Day 14 was accompanied by significant upregulation of ALP and OC expressions on Days 14 and 28. This was expected, because OSX is an early osteogenic transcription factor that lies downstream of runt-related transcription factor 2 (Runx2) and stimulates bone matrix deposition and mineralization through elevated levels of collagen type I, ALP and OC[70].

Attachment of DPSCs on the substrates

Cell numbers on the substrates 16 h after seeding given in Fig.3A showed a lower number of cells attached on the substrates than the TCPS control. Meanwhile, a significantly higher number of cells attached on the patterned surfaces compared to the unpatterned control in the untreated group indicated a positive effect of micropillars on cell attachment. Enhanced cell attachment by micropillars was reported earlier for astrocytes[71], cardiomyocytes[72], and MSCs[26, 73], which can be attributed to larger contact area[73] and better formation and maturation of focal adhesions[74] assisted by 3D patterns. Despite the decrease in wettability with a decrease in pillar and gap length, cell attachment was higher on P4G4 than on P8G8 and P16G16. This observation cannot be explained with increased contact as all patterned surfaces used in this study had geometrically the same total surface area. Higher cell attachment on P4G4 was probably a result of the highest number of pillars per unit area that a cell can interact, considering that the edges of pillar tops were shown to be where focal contacts were mainly concentrated on[75].

Oxygen plasma treatment dramatically increased cell attachment on all surfaces but P4G4. Cell attachment on the plasma treated surfaces increased with increasing pillar and gap width, from P4G4 towards P16G16, possibly because of the larger interpillar gaps being able to accommodate more cells. The increase in cell attachment upon plasma treatment can be attributed to the change of profile and conformation of adsorbed proteins with an increase in hydrophilicity as well as the nano-roughening of the surfaces due to plasma etching[64]. A positive effect of oxygen plasma treatment on cell attachment was also reported before by others[76, 77]. In those studies, WCA were in the range 40°−70°, which is generally accepted

to be optimum for mammalian cell adhesion on polymeric surfaces[78]. The range of WCA of the plasma treated surfaces used in this study, however, was much lower (between 10–20°)[51] and cell attachment was still very high compared to untreated counterparts. Similar observations of significantly improved cell attachment on extremely wettable surfaces were also reported with nerve cells and osteoblasts on oxygen plasma treated poly(l-lactic acid) (PLLA)[79] and hexamethyldisiloxane surfaces[80], respectively. Our findings and those of others indicate that the optimal wettability for cell attachment is not a fixed value but rather vary with the material and cell type, and treatment conditions.

Positioning and morphology of DPSCs on the substrates

Lateral dimensions and hydrophilicity of the micropillars determined the relative positions and morphology of DPSCs as can be seen in SEM micrographs given in Fig.3B (lower magnification in Fig.S5). Cells on the untreated smooth surfaces (Fig.3B-i) did not spread well while the cells on the O_2 plasma treated counterparts (Fig.3B-v) did with numerous extensions. On the untreated P4G4 and P8G8 surfaces, most of the cell bulk was located on pillar tops (Fig.3B-ii, iii), forming bridges over the interpillar spaces and extending their filopodia downward to the substrate floor. On the plasma treated counterparts (Fig.3B-vi, vii), on the other hand, cells were localized on the substrate floor with their filopodia extended towards and stretched over the pillar tops. Cells on both the untreated and the plasma treated P16G16 surfaces (Fig.3B-iv, viii) were spread in the interpillar gaps.

Confocal microscopy images of the cells presented in Fig.4A shows the distinct changes in cell and nucleus morphology. Cells were squeezed between the pillars and conformed their cytoplasm to the interpillar spaces, constraining their typical spread morphology seen on the unpatterned surface. Cells were extremely elongated on P4G4 but highly branched on P8G8 and P16G16 surfaces. Same trends in cell morphology were also observed on the plasma treated surfaces. Cells were localized more in the interpillar spaces and surround the pillars on plasma treated P8G8 and P16G16 substrates. Together with cell bodies, nuclei were also inserted between the pillars and distorted on patterned surfaces, particularly on P4G4 (Fig. 4B). Interestingly, cells that were located in between the pillars of untreated P4G4 and P8G8 (Fig.S6) surfaces on Day 7 crawled back on top of the pillars on Day 14 and showed no significant nuclear deformation. On the oxygen plasma treated counterparts, however, majority of the cells were still squeezed in between the pillars and had deformed nuclei on Day 14.

Cell proliferation on the substrates

Both micropatterns and plasma modification had a profound effect on cell proliferation on the substrates (Fig.5A). Cell numbers (Fig.S7) on untreated P8G8 and P16G16 surfaces were comparable with that on the unpatterned control, while there were significantly lower number of cells on P4G4 surface at all time points. Cell numbers on oxygen plasma treated substrates were significantly higher than those on untreated counterparts throughout 21 days of culture, but P4G4 surface still had less cells than unpatterned or P8G8 and P16G16 surfaces on Days 3 and 7. Oxygen plasma treatment and larger pillar/gap widths were found to increase proliferation rate on the substrates between days 3 and 7. The positive effect of oxygen plasma modification on cell division was also reported by others[81, 82] and it can be

attributed to the introduction of oxygen-rich groups such as hydroxyl and carboxylic acid, which were shown to modulate protein adsorption and subsequent transmission of proliferative signals mediated by integrin-ligand interactions[83]. After Day 7, specific growth rates on plasma treated surfaces decreased compared to the earlier time intervals and became lower than those on the untreated substrates (Supplementary Table 3), probably because of contact inhibition[84] after reaching confluency.

Considering the increase in nuclear deformations and decrease in proliferation rates with a decrease in pillar and gap size from P16G16 towards P4G4, a negative effect of nuclear deformations on cell proliferation can be suggested, particularly at early time points. Mitosis is a highly organized process that involves precise and predetermined rearrangements of genetic material in the nucleus; therefore, severe deformations in the nuclei might interrupt cell division by obstructing the access of the replication machinery to DNA[85]. Indeed, a negative correlation was found between the specific growth rates and the average nuclear deformation values on the substrates during Days 3–7 (Fig.5B). Nagayama et al. also reported inhibition of the proliferation of vascular smooth muscle cells on micropillar decorated surfaces, which they explained by the condensation of the chromatin in the deformed nuclei[33]. Specific growth rates between days 7 and 14 on untreated P4G4 and P8G8 surfaces leveled with those on the unpatterned and P16G16 surfaces (Supplementary Table 3), probably because of the gradual disappearance of nuclear deformations on P4G4 and P8G8 as the cells crawled onto the pillar tops at later time points.

Expression of osteogenic marker genes on the substrates

Micropillar arrays on which distinct changes were observed in cytoskeletal and nuclear morphologies led to alterations in gene expression (Fig. 6A–C) as expected. On Day 7, OSX expression was 2-fold higher on the untreated P4G4 and P8G8 but not on P16G16. However, the relative expression of OSX on P4G4 and P8G8 surfaces levelled down to the baseline on Days 14 and 28. The early upregulation of OSX on P4G4 and P8G8 surfaces was followed by approximately 4-fold and 6-fold increases in ALP expression on Days 14 and 28, respectively. The ALP levels on untreated P4G4 and P8G8 on Day 14 were higher than that was obtained with chemical induction (Fig.2B), suggesting that the commitment to osteogenic lineage was triggered by surface patterns earlier than with soluble factors. Unlike chemical induction, however, the expression of OC on untreated micropillar arrays did not change significantly over 28 days of culture. OC is a relatively late osteogenic marker[86] and was shown before to be expressed later than ALP during osteogenesis[87, 88], indicating that micropillar arrays might have induced osteogenesis earlier than by chemicals but did not lead to a mature osteoblastic phenotype over the 4 weeks of culture. Gene expression at later time points should be analyzed to investigate whether a fully mature osteoblast phenotype can be achieved on the patterned surfaces. In this case, the time that cells spend in between the micropillar features could be increased by delaying confluency by decreasing the initial number of cells seeded.

Interestingly, no significant change was observed in the expression of osteogenic marker genes on the oxygen plasma treated substrates during the first 2 weeks of culture (Fig.6A–C, hatched columns). The only significant change was the upregulation of OSX on P4G4 and

P8G8 surfaces on Day 28, suggesting a much later commitment to osteogenesis on the plasma treated substrates. Our hypothesis was that cytoskeletal tensions due to the micropillar mediated morphological changes and nuclear deformations could trigger osteogenesis. Considering earlier and more robust morphological changes we reported before on the oxygen plasma treated micropillar arrays[51], we were expecting the cells on such surfaces to differentiate earlier. An explanation to this situation could be the initial high proliferation rates on the plasma treated surfaces as summarized in Supplementary Table 4. Cell cycle withdrawal and differentiation are coupled processes; differentiating cells need a longer cell cycle to respond to external signals and to accumulate differentiation-inducing transcription factors, resulting in a decrease in proliferation rate[89, 90]. For example, pre-osteoblastic cells differentiated by forced upregulation of Runx2 and OSX were shown to suspend cell cycle, resulting in a transition from active cell growth to quiescence[91]. Significantly higher initial proliferation rates we recorded on plasma treated surfaces point out to shorter cell cycles, which might have prevented cells from getting into a differentiation state. The influence of cellular shape on the expression of osteogenic genes was investigated by correlation test. Surface topography-induced elongation of MSCs was reported by others to enhance osteogenesis by chemical induction[37, 92, 93]. This was later explained with the upregulation of OSX via reorganization of cytoskeletal elements and following signaling cascades on patterned surfaces[95–97]. Here, on the untreated surfaces, we found no correlation between cell elongation (observed on P4G4) or branching (observed on P8G8 and P16G16) and OSX expression (Supplementary Table 5, Fig.S8A). This finding suggests that cytoskeletal tension resulting from changes in cell morphology in the forms of elongation or branching modulates osteogenesis on patterned substrates.

It is noteworthy that OSX and ALP were upregulated on P4G4 and P8G8 but not on P16G16, implying an effect of nuclear deformation on osteogenesis. Deviations from the elliptical shape of cell nucleus was proposed as one of the factors altering structure and organization of chromatin and therefore modulating gene expression[98]. Osteogenic genes including OSX, ALP and OC were shown to be located within the telomeric regions of large chromosomes, which were predisposed to repositioning upon intranuclear reorganization[18]. Indeed, we found a positive correlation between OSX and ALP expressions and the extent of nuclear deformations (Supplementary Table 6, Fig.S8B). Liu et al. reported earlier that nuclear deformations on micropillars significantly enhanced the expressions of Runx2 and ALP by MSCs cultured in a cocktail of osteogenic and adipogenic supplements[38]. Here we report a similar observation but without chemical induction.

Bone extracellular matrix deposition and mineralization

Immunofluorescence was used to detect deposition of bone ECM proteins, collagen type I (COL I) and osteopontin (OP), in response to physical cues (Fig. 7A). Cells on untreated substrates, particularly those on micropillar decorated surfaces, were found to aggregate into osteogenic nodule-like structures rich in COL I and OP. Cells on the plasma treated surfaces, however, were well spread and did not form aggregates. A few large aggregates were observed on P4G4 while there were multiple, denser aggregates on P8G8 and P16G16. Human MSCs undergoing osteogenic differentiation are known to form multilayered nodular structures *in vitro*[99, 100], and hydrophobic substrates were shown before to force

stem cells to aggregate and enhance osteogenesis[101]. Contrary to a previous report of aggregate formation on nano but not on micropillars[102], our substrates triggered formation of bone nodule-like aggregations.

The deposition of COL I and OP were semi-quantified in Fig.7B and Fig.7C, respectively, by normalization of fluorescence intensities to nuclear signal. Plasma modification was found to increase COL I and OP deposition on unpatterned surfaces. Moreover, normalized intensities of COL I and OP were lower on both untreated and plasma treated micropillar arrays compared to the unpatterned control surfaces. These observations suggest that bone matrix deposition increase with increasing cell spreading. We previously showed that oxygen plasma modification increases cell spread area on unpatterned surfaces. It can also clearly be seen that cell spreading is significantly restricted on micropillar decorated surfaces, particularly on untreated hydrophobic substrates. Indeed, synthesis and deposition of COL I were shown to increase with increasing cell spreading even if the levels of pro-α1(I) collagen mRNA were the same[103]. COL I deposition was higher on the untreated micropillar arrays except P8G8 than their plasma treated counterparts, while OP deposition was higher on plasma treated substrates (except P16G16). Surface hydrophilicity was shown to enhance deposition of OP both *in vitro*[104] and *in vivo*[105] because of higher BMP signaling on hydrophilic surfaces.

The nodular aggregates on untreated P4G4 and P8G8 surfaces were found to be positive for calcium deposits by Alizarin red staining (Fig. 8, shown with yellow arrows), indicating mineralization. Only a low basal staining was observed on the plasma treated counterparts, indicating no significant mineralization over 28 days of culture. Higher deposition of COL-I and OP on plasma treated surfaces but lack of mineralization may look contradictory considering that bone matrix proteins promote mineralization. However, it should be noted that mineralization was observed on untreated P4G4 and P8G8 surfaces, where cell bone nodule-like aggregates were positive for both COL-I and OP, and the expression of ALP was significantly upregulated on days 14 and 28 following the early upregulation of OSX on Day 7. On plasma treated P4G4 and P8G8 surfaces, on the other hand, no significant change was observed in ALP levels compared to the unpatterned control over 28 days of culture. Upregulation of ALP is essential for bone mineralization since it promotes calcium phosphate deposition by increasing the local concentrations of inorganic phosphate and decreasing the levels of extracellular pyrophosphate, which is known to inhibit mineralization[107].

Overall, our findings indicate that square prism micropillars cause significant alterations in cytoskeletal and nuclear morphology and induce upregulation of early osteogenic genes and mineralization on hydrophobic PMMA surfaces. We propose that sharp edges of the square prism pillars and narrow interpillar gaps on P4G4 and P8G8 substrates generated high degrees of cytoskeletal tension and induced differentiation of multipotent DPSCs towards bone lineage rather than soft tissue cells such as adipocytes. It was previously shown that MSCs grown on adhesive microislands with sharp corners and curvature in the shape of rectangles or stars induced osteogenesis while the cells on smoother patterns like round islands or flowers underwent adipogenic differentiation[92]. Besides the nature of morphological changes, high stiffness of the solvent-cast PMMA films probably favored

differentiation towards osteogenesis rather than adipogenesis or myogenesis. Considering the influence of matrix stiffness on lineage commitment of MSCs[108], the elastic modulus of our solvent cast PMMA films (~1.3 GPa[52]) was far too high for adipogenic (1–5 kPa) or myogenic (10–20 kPa) differentiation but favors osteogenesis (>25 kPa)[109].

Conclusions

In this study, PMMA micropillar arrays with varying lateral dimensions were fabricated and their wettability was improved by treating with oxygen plasma. These micropillar structures were shown to affect morphologies of cell body and nucleus, and modulate attachment, proliferation and osteogenic differentiation of DPSCs. Hydrophobic micropillar arrays with lateral dimensions of 4 (P4G4) and 8 μm (P8G8) induced the expression of early osteogenic genes and mineralization in bone nodule-like cell aggregates without any differentiation supplements in the growth media. In conclusion we propose that hydrophobic square prism micropillars bring osteoinduction to PMMA surfaces without biochemical supplements. Our approach is more advantageous over other methods employing nanoscale patterns that require more complicated and costly methods for fabrication[9] or using materials such as genetically engineered proteins[55] or decellularized bone matrices[106] that are harder to process. Hence, P4G4 and P8G8 surfaces have significant potential for use of biomaterial topographies as a safer alternative to soluble factors in inducing the osteogenic differentiation of mesenchymal stem cells and as a result for more effective bone implants. Future studies will focus on the expression of bone marker genes at later time points to determine whether osteogenesis is fully induced also on the plasma treated surfaces and whether a fully mature osteoblast phenotype can be achieved on the untreated hydrophobic substrates without chemical induction. Besides potential applications on the surface of bone biomaterials, our strategy to induce cell differentiation by modulation of cellular morphology on micropillar decorated surfaces can also be employed in tissue engineering applications with biodegradable polymers such as poly(L-lactic acid) (PLLA) or poly(lactic-co-glycolic acid) (PLGA) using the same approach [45]. Multilayered 3D scaffolds can also be constructed by stacking individual micropillar decorated films on top of each other[110]. Moreover, the strategy can be expanded to investigate myogenic differentiation due to the extensive cell elongation observed on P4G4 surfaces but by using softer materials such as collagen[46].

Supplementary Material

Refer to Web version on PubMed Central for supplementary material.

Acknowledgements

OH, ME, NH and VH acknowledge Middle East Technical University (METU) Center of Excellence in Biomaterials and Tissue Engineering (BIOMATEN) for the use of the facilities, Prof. Ercument Onder of METU Health Center Department of Dentistry for the extraction of human dental pulp tissues, METU Central Laboratory for SEM analyses, and the financial support from the Ministry of Development of Turkey (METU BAP-01-08-2013-003 and BAP-08-11-DPT2011K120350). OH and ME also acknowledge TUBITAK 2210-E and 2211-C scholarships, respectively. UD would like to acknowledge NIH R15HL115556, NSF CAREER Award Number 1461602 and NSF EAGER 1547791.

References

[1]. Zhou H; Lee J Nanoscale hydroxyapatite particles for bone tissue engineering. Acta Biomater. 2011, 7, 2769–2781. [PubMed: 21440094]

[2]. Liu Y; Lim J; Teoh SH Review: development of clinically relevant scaffolds for vascularised bone tissue engineering. Biotechnol. Adv 2013, 31, 688–705. [PubMed: 23142624]

[3]. Shrivats AR; McDermott MC; Hollinger JO Bone tissue engineering: state of the union. Drug Discov. Today 2014, 19, 781–786. [PubMed: 24768619]

[4]. Stock UA; Vacanti JP Tissue engineering: current state and prospects. Annu. Rev. Med 2001, 52, 443–451. [PubMed: 11160788]

[5]. Gronthos S; Mankani M; Brahim J; Robey PG; Shi S Postnatal human dental pulp stem cells (DPSCs) in vitro and in vivo. Proc. Natl. Acad. Sci. U.S.A 2000, 97, 13625–13630. [PubMed: 11087820]

[6]. Perry BC; Zhou D; Wu X; Yang FC; Byers MA; Chu TMG; Goebel WS Collection, cryopreservation, and characterization of human dental pulp-derived mesenchymal stem cells for banking and clinical use. Tissue Eng. Part C Methods 2008, 14, 149–156. [PubMed: 18489245]

[7]. Lee K; Silva EA; Mooney DJ Growth factor delivery-based tissue engineering: general approaches and a review of recent developments. J. R. Soc. Interface 2011, 8, 153–170. [PubMed: 20719768]

[8]. Anderson JM; Vines JB; Patterson JL; Chen H; Javed A; Jun HW Osteogenic differentiation of human mesenchymal stem cells synergistically enhanced by biomimetic peptide amphiphiles combined with conditioned medium. Acta Biomater. 2011, 7, 675–682. [PubMed: 20728586]

[9]. Martinez E; Engel E; Planell JA; Samitier J Effects of artificial micro-and nano-structured surfaces on cell behavior. Ann. Anat 2009, 191, 126–135. [PubMed: 18692370]

[10]. Edalat F; Bae H; Manoucheri S; Cha JM; Khademhosseini A Engineering approaches toward deconstructing and controlling the stem cell environment. Ann. Biomed. Eng 2012, 40, 1301–1315. [PubMed: 22101755]

[11]. Lv L; Tang Y; Zhang P; Liu Y; Bai X; & Zhou Y Biomaterial cues regulate epigenetic state and cell functions—A systematic review. Tissue Eng. Part B Rev. 2018, 24, 112–132. [PubMed: 28903618]

[12]. Vogel V; Sheetz M Local force and geometry sensing regulate cell functions. Nat. Rev. Mol. Cell Biol 2006, 7, 265–275. [PubMed: 16607289]

[13]. Wang YK; Yu X; Cohen DM; Wozniak MA; Yang MT; Gao L; Chen CS Bone morphogenetic protein-2-induced signaling and osteogenesis is regulated by cell shape, RhoA/ROCK, and cytoskeletal tension. Stem Cells Dev. 2012, 21, 1176–1186. [PubMed: 21967638]

[14]. Zhou X; Novotny JE; Wang L Anatomic variations of the lacunar–canalicular system influence solute transport in bone. Bone 2009, 45, 704–710. [PubMed: 19576310]

[15]. Bhadriraju K; Yang M; Ruiz SA; Pirone D; Tan J; Chen CS Activation of ROCK by RhoA is regulated by cell adhesion, shape, and cytoskeletal tension. Exp. Cell. Res 2007, 313, 3616–3623. [PubMed: 17673200]

[16]. Burridge K; Guilluy C Focal adhesions, stress fibers and mechanical tension. Exp. Cell Res 2016, 343, 14–20. [PubMed: 26519907]

[17]. Anselme K; Wakhloo NT; Rougerie P; Pieuchot L Role of the Nucleus as a Sensor of Cell Environment Topography. Adv. Healthc. Mater 2018, 7, 1701154.

[18]. McNamara LE; Burchmore R; Riehle MO; Herzyk P; Biggs MJ; Wilkinson CD; Dalby MJ The role of microtopography in cellular mechanotransduction. Biomaterials 2012, 33, 2835–2847. [PubMed: 22248989]

[19]. Lozoya OA; Gilchrist CL; Guilak F Universally conserved relationships between nuclear shape and cytoplasmic mechanical properties in human stem cells. Sci. Rep 2016, 6, 23047. [PubMed: 26976044]

[20]. Thorpe SD; Lee DA Dynamic regulation of nuclear architecture and mechanics—a rheostatic role for the nucleus in tailoring cellular mechanosensitivity. Nucleus 2017, 0, 1–14.

[21]. Voldman J; Gray ML; Schmidt MA Microfabrication in biology and medicine. Annu. Rev. Biomed. Eng 1999, 1, 401–425. [PubMed: 11701495]

[22]. Ermis M; Antmen E; Hasirci V Micro and Nanofabrication methods to control cell-substrate interactions and cell behavior: A review from the tissue engineering perspective. Bioact. Mater, 2018, 3(3), 355–369. [PubMed: 29988483]

[23]. Hasirci V; Kenar H Novel surface patterning approaches for tissue engineering and their effect on cell behavior. Future Med 2006, 1, 73–90.

[24]. Hasirci V; Pepe-Mooney BJ Understanding the cell behavior on nano-/micro-patterned surfaces. Nanomedicine 2012, 7, 1375–1389. [PubMed: 22812706]

[25]. Dalby MJ; Gadegaard N; Riehle MO; Wilkinson CD; Curtis AS Investigating filopodia sensing using arrays of defined nano-pits down to 35 nm diameter in size. Int. J. Biochem. Cell Biol 2004, 36, 2005–2015. [PubMed: 15203114]

[26]. Kolind K; Kraft D; Bøggild T; Duch M; Lovmand J; Pedersen FS; Besenbacher F Control of proliferation and osteogenic differentiation of human dental-pulp-derived stem cells by distinct surface structures. Acta Biomater 2014, 10, 641–650. [PubMed: 24252446]

[27]. Mai J; Sun C; Li S; Zhang X; A microfabricated platform probing cytoskeleton dynamics using multidirectional topographical cues. Biomed. Microdevices 2007, 9, 523–531. [PubMed: 17516174]

[28]. Jeon H; Hidai H; Hwang DJ; Healy KE; Grigoropoulos CP The effect of micronscale anisotropic cross patterns on fibroblast migration. Biomaterials 2010, 31, 4286–4295. [PubMed: 20189640]

[29]. Andersson AS; Olsson P; Lidberg U; Sutherland D The effects of continuous and discontinuous groove edges on cell shape and alignment. Exp. Cell. Res 2003, 288, 177–188. [PubMed: 12878169]

[30]. Ghibaudo M; Trichet L; Le Digabel J; Richert A; Hersen P; Ladoux B Substrate topography induces a crossover from 2D to 3D behavior in fibroblast migration. Biophys. J 2009, 97, 357–368. [PubMed: 19580774]

[31]. Hamilton DW; Wong KS; Brunette DM Microfabricated discontinuous-edge surface topographies influence osteoblast adhesion, migration, cytoskeletal organization, and proliferation and enhance matrix and mineral deposition in vitro. Calcif. Tissue Int 2006, 78, 314–325. [PubMed: 16604286]

[32]. Moroni L; Lee LP Micropatterned hot- embossed polymeric surfaces influence cell proliferation and alignment. J. Biomed. Mater. Res. A 2009, 88, 644–653. [PubMed: 18314900]

[33]. Nagayama K; Hamaji Y; Sato Y; Matsumoto T Mechanical trapping of the nucleus on micropillared surfaces inhibits the proliferation of vascular smooth muscle cells but not cervical cancer HeLa cells. J. Biomech 2015, 48, 1796–1803. [PubMed: 26054426]

[34]. Dalby MJ; Gadegaard N; Tare R; Andar A; Riehle MO; Herzyk P; Oreffo RO The control of human mesenchymal cell differentiation using nanoscale symmetry and disorder. Nat. Mater 2007, 6, 997–1003. [PubMed: 17891143]

[35]. Lovmand J; Justesen J; Foss M; Lauridsen RH; Lovmand M; Modin C; Besenbachera F; Pedersen FS; Duch M The use of combinatorial topographical libraries for the screening of enhanced osteogenic expression and mineralization. Biomaterials 2009, 30, 2015–2022. [PubMed: 19178942]

[36]. McNamara LE; McMurray RJ; Biggs MJ; Kantawong F; Oreffo RO; Dalby MJ Nanotopographical control of stem cell differentiation. J. Tissue Eng 2010, 1, 120623.

[37]. Abagnale G; Steger M; Nguyen VH; Hersch N; Sechi A; Joussen S; Schnakenberg U Surface topography enhances differentiation of mesenchymal stem cells towards osteogenic and adipogenic lineages. Biomaterials 2015, 61, 316–326. [PubMed: 26026844]

[38]. Liu X; Liu R; Cao B; Ye K; Li S; Gu Y; Ding J Subcellular cell geometry on micropillars regulates stem cell differentiation. Biomaterials 2016, 111, 27–39. [PubMed: 27716524]

[39]. Curtis A; Wilkinson C Topographical control of cells. Biomaterials 1997, 18, 1573–1583. [PubMed: 9613804]

[40]. Kenar H; Kocabas A; Aydinli A; Hasirci V Chemical and topographical modification of PHBV surface to promote osteoblast alignment and confinement. J. Biomed. Mater. Res. A 2008, 85, 1001–1010. [PubMed: 17907245]

[41]. Ozcelik H; Padeste C; Hasirci V Systematically organized nanopillar arrays reveal differences in adhesion and alignment properties of BMSC and Saos-2 cells. Colloids Surf. B 2014, 119, 71–81.

[42]. Alapan Y; Younesi M; Akkus O; Gurkan UA Anisotropically stiff 3D micropillar niche induces extraordinary cell alignment and elongation. Adv. Healthc. Mater 2016, 5, 1884–1892. [PubMed: 27191679]

[43]. Muhammad R; Peh GS; Adnan K; Law JB; Mehta JS; Yim EK Micro-and nano-topography to enhance proliferation and sustain functional markers of donor-derived primary human corneal endothelial cells. Acta Biomater 2015, 19, 138–148. [PubMed: 25796353]

[44]. Carvalho A; Pelaez-Vargas A; Hansford DJ; Fernandes MH; Monteiro FJ Effects of line and pillar array microengineered SiO2 thin films on the osteogenic differentiation of human bone marrow-derived mesenchymal stem cells. Langmuir 2016, 32, 1091–1100. [PubMed: 26771563]

[45]. Ermis M; Akkaynak D; Chen P; Demirci U; Hasirci V A high throughput approach for analysis of cell nuclear deformability at single cell level. Sci. Rep 2016, 6, 36917. [PubMed: 27841297]

[46]. Antmen E; Ermis M; Demirci U; Hasirci V Engineered natural and synthetic polymer surfaces induce nuclear deformation in osteosarcoma cells. J. Biomed. Mater. Res. B, 2018, 00B, 000–000.

[47]. Pan Z; Yan C; Peng R; Zhao Y; He Y; Ding J Control of cell nucleus shapes via micropillar patterns. Biomaterials 2012, 33, 1730–1735. [PubMed: 22133552]

[48]. Liu X; Liu R; Gu Y; Ding J Non-Monotonic self-deformation of cell nuclei on topological surfaces with micropillar array. ACS Appl. Mater. Interfaces 2017, 9, 18521–19530. [PubMed: 28514142]

[49]. Liu R; Liu Q; Pan Z; Liu X; Ding J Cell-type and nuclear-size dependence of nuclear deformation of cells on a micropillar array. Langmuir. 2018.

[50]. Grespan E; Giobbe GG; Badique F; Anselme K; Rühe J; Elvassore N Effect of geometrical constraints on human pluripotent stem cell nuclei in pluripotency and differentiation. Integr. Biol 2018, 10, 278–289.

[51]. Hasturk O; Sivas A; Karasozen B; Demirci U; Hasirci N; Hasirci V Quantification of type, timing, and extent of cell body and nucleus deformations caused by the dimensions and hydrophilicity of square prism micropillars. Adv.Healthc. Mat 2016, 5, 2972–2982.

[52]. Hasturk O; Ermis M; Demirci U; Hasirci N; Hasirci V Square prism micropillars improve osteogenicity of poly(methyl methacrylate) surfaces. J. Mater. Sci. Mater. Med, 2018, 29(5), 53. [PubMed: 29721618]

[53]. Peng R; Yao X; Cao B; Tang J; Ding J The effect of culture conditions on the adipogenic and osteogenic inductions of mesenchymal stem cells on micropatterned surfaces. Biomaterials 2012, 33, 6008–6019. [PubMed: 22681981]

[54]. Yao X; Peng R; Ding J Cell–material interactions revealed via material techniques of surface patterning. Adv. Mater 2013, 25, 5257–5286. [PubMed: 24038153]

[55]. Wang J; Wang L; Li X; Mao C Virus activated artificial ECM induces the osteoblastic differentiation of mesenchymal stem cells without osteogenic supplements. Scientific reports, 2013, 3, 1242. [PubMed: 23393624]

[56]. Yang M; Shuai Y; Sunderland KS; Mao C Ice- Templated Protein Nanoridges Induce Bone Tissue Formation. Adv. Funct. Mater, 2017, 27(44), 1703726. [PubMed: 29657571]

[57]. Watari S; Hayashi K; Wood JA; Russell P; Nealey PF; Murphy CJ; Genetos DC Modulation of osteogenic differentiation in hMSCs cells by submicron topographically-patterned ridges and grooves. Biomaterials 2012, 33, 128–136. [PubMed: 21982295]

[58]. Khanna-Jain R; Vanhatupa S; Vuorinen A; Sandor GK; Suuronen R; Mannerstrom B; Miettinen S Growth and differentiation of human dental pulp stem cells maintained in fetal bovine serum, human serum and serum-free/xeno-free culture media. J. Stem Cell Res. Ther 2012, 2, 1–11. [PubMed: 23482850]

[59]. Schop D; Janssen FW; van Rijn LD; Fernandes H; Bloem RM; de Bruijn JD; van Dijkhuizen-Radersma R Growth, metabolism, and growth inhibitors of mesenchymal stem cells. Tissue Eng Part A., 2009, 15(8), 1877–1886. [PubMed: 19196147]

[60]. Schmittgen TD; Livak KJ Analyzing real-time PCR data by the comparative CT method. Nat. Protoc 2008, 3, 1101–1108. [PubMed: 18546601]

[61]. Arima Y; Iwata H Effect of wettability and surface functional groups on protein adsorption and cell adhesion using well-defined mixed self-assembled monolayers. Biomaterials 2007, 28, 3074–3082. [PubMed: 17428532]

[62]. Jeon H; Lee H; Kim G A surface-modified poly (ε-caprolactone) scaffold comprising variable nanosized surface-roughness using a plasma treatment. Tissue Eng. Part C Methods 2014, 20, 951–963. [PubMed: 24635019]

[63]. Hasirci V; Tezcaner A; Hasirci N; Suzer S Oxygen plasma modification of poly(3-hydroxybutyrate- co- 3- hydroxyvalerate) film surfaces for tissue engineering purposes. J. Appl. Polym. Sci, 2003, 87, 1285–1289.

[64]. Ozcan C; Hasirci N Plasma modification of PMMA films: surface free energy and cell-attachment studies. J. Biomater. Sci. Polym. Ed 2007, 18, 759–773. [PubMed: 17623556]

[65]. Yildirim S In Dental Pulp Stem Cells. Springer Verlag: New York, NY, 2013, Chapter 5, pp. 41–51.

[66]. Mokry J; Soukup T; Micuda S; Karbanova J; Visek B; Brcakova E; Suchanek J; Bouchal J; Vokurkova D; Ivancakova R Telomere attrition occurs during ex vivo expansion of human dental pulp stem cells. J. Biomed. Biotechnol 2010, 2010, 673513. [PubMed: 20976265]

[67]. Kanafi MM; Ramesh A; Gupta PK; Bhonde RR Influence of hypoxia, high glucose, and low serum on the growth kinetics of mesenchymal stem cells from deciduous and permanent teeth. Cells Tissues Organs 2013, 198, 198–208. [PubMed: 24192068]

[68]. Ibarretxe GO; Crende M; Aurrekoetxea V; García-Murga J; Etxaniz FU Neural crest stem cells from dental tissues: a new hope for dental and neural regeneration. Stem Cells Int. 2012, 2012, 103503. [PubMed: 23093977]

[69]. Igarashi M; Kamiya N; Hasegawa M; Kasuya T; Takahashi T; Takagi M Inductive effects of dexamethasone on the gene expression of Cbfa1, Osterix and bone matrix proteins during differentiation of cultured primary rat osteoblasts. J. Mol. Histol 2004, 35, 3–10. [PubMed: 15323344]

[70]. Nakashima K; Zhou X; Kunkel G; Zhang Z; Deng JM; Behringer RR; de Crombrugghe B The novel zinc finger-containing transcription factor osterix is required for osteoblast differentiation and bone formation. Cell 2002, 108, 17–29. [PubMed: 11792318]

[71]. Craighead HG; Turner SW; Davis RC; James C; Perez AM; John PS; Banker G Chemical and topographical surface modification for control of central nervous system cell adhesion. Biomed. Microdevices 1998, 1, 49–64.

[72]. Deutsch J; Motlagh D; Russell B; Desai TA Fabrication of microtextured membranes for cardiac myocyte attachment and orientation. J. Biomed. Mater. Res. A 2000, 53, 267–275.

[73]. Su WT; Liao YF; Lin CY; Li LT Micropillar substrate influences the cellular attachment and laminin expression. J. Biomed. Mater. Res. A 2010, 93, 1463–1469. [PubMed: 19967757]

[74]. Liang EI; Mah EJ; Yee AF; Digman MA Correlation of focal adhesion assembly and disassembly with cell migration on nanotopography. Integr. Biol 2017, 9, 145–155.

[75]. Seo CH; Furukawa K; Montagne K; Jeong H; Ushida T The effect of substrate microtopography on focal adhesion maturation and actin organization via the RhoA/ROCK pathway. Biomaterials 2011, 32, 9568–9575. [PubMed: 21925729]

[76]. Ozcan C; Zorlutuna P; Hasirci V; Hasirci N Influence of oxygen plasma modification on surface free energy of PMMA films and cell attachment. Macromol. Symp 2008, 269, 128–137.

[77]. Borges AMG; Benetoli LO; Licínio MA; Zoldan VC; Santos-Silva MC; Assreuy J; Soldi V Polymer films with surfaces unmodified and modified by non-thermal plasma as new substrates for cell adhesion. Mater. Sci. Eng. C Mater. Biol. Appl 2013, 33, 1315–1324. [PubMed: 23827577]

[78]. Saltzman WM; Kyriakides TR In Principles of Tissue Engineering, 3rd ed; Lanza R, Langer R, Vacanti JP, Eds.; Academic Press: New York, NY, 2000; Chapter 20, pp 279–297.

[79]. Khorasani MT; Mirzadeh H; Irani S Plasma surface modification of poly (L-lactic acid) and poly (lactic-co-glycolic acid) films for improvement of nerve cells adhesion. Radiat. Phys. Chem 2008, 77, 280–287.

[80]. Wei J; Igarashi T; Okumori N; Igarashi T; Maetani T; Liu B; Yoshinari M Influence of surface wettability on competitive protein adsorption and initial attachment of osteoblasts. Biomed. Mater 2009, 4, 045002. [PubMed: 19525576]

[81]. Kim SH; Ha HJ; Ko YK; Yoon SJ; Rhee JM; Kim MS; Khang G Correlation of proliferation, morphology and biological responses of fibroblasts on LDPE with different surface wettability. J. Biomater. Sci. Polym. Ed 2007, 18, 609–622. [PubMed: 17550662]

[82]. Mirmohammadi SA; Khorasani MT; Mirzadeh H; Irani S Investigation of plasma treatment on poly (3-hydroxybutyrate) film surface: characterization and invitro assay. Polym. Plast. Technol. Eng 2012, 51, 1319–1326.

[83]. Ma Z; Gao C; Gong Y; Shen J Chondrocyte behaviors on poly-L-lactic acid (PLLA) membranes containing hydroxyl, amide or carboxyl groups. Biomaterials 2003, 24, 3725–3730. [PubMed: 12818544]

[84]. Polyak K; Kato JY; Solomon MJ; Sherr CJ; Massague J; Roberts JM; Koff A p27Kip1, a cyclin-Cdk inhibitor, links transforming growth factor-beta and contact inhibition to cell cycle arrest. Genes Dev. 1994, 8, 9–22. [PubMed: 8288131]

[85]. Roca-Cusachs P; Alcaraz J; Sunyer R; Samitier J; Farré R; Navajas D Micropatterning of single endothelial cell shape reveals a tight coupling between nuclear volume in G1 and proliferation. Biophys. J 2008, 94, 4984–4995. [PubMed: 18326659]

[86]. Zoch ML; Clemens TL; Riddle RC New insights into the biology of osteocalcin. Bone, 2016, 82, 42–49. [PubMed: 26055108]

[87]. Stein GS; Lian JB Molecular mechanisms mediating proliferation/differentiation interrelationships during progressive development of the osteoblast phenotype. Endocr. Rev 1993, 14, 424–442. [PubMed: 8223340]

[88]. Kato Y; Boskey A; Spevak L; Dallas M; Hori M; Bonewald LF Establishment of an osteoid preosteocyte- like cell mlo- a5 that spontaneously mineralizes in culture. J. Bone Miner. Res, 2001, 16(9), 1622–1633. [PubMed: 11547831]

[89]. Constantinescu D; Gray HL; Sammak PJ; Schatten GP; Csoka AB Lamin A/C expression is a marker of mouse and human embryonic stem cell differentiation. Stem cells 2006, 24, 177–185. [PubMed: 16179429]

[90]. Pajerowski JD; Dahl KN; Zhong FL; Sammak PJ; Discher DE Physical plasticity of the nucleus in stem cell differentiation. Proc. Natl. Acad. Sci. U.S.A 2007, 104, 15619–15624. [PubMed: 17893336]

[91]. Jaiswal N; Haynesworth SE; Caplan AI; Bruder SP Osteogenic differentiation of purified, culture- expanded human mesenchymal stem cells in vitro. J. Cell. Biochem 1997, 64, 295–312. [PubMed: 9027589]

[92]. Kilian KA; Bugarija B; Lahn BT; Mrksich M Geometric cues for directing the differentiation of mesenchymal stem cells. Proc. Natl. Acad. Sci. U.S.A 2010, 107, 4872–4877. [PubMed: 20194780]

[93]. Yao X; Peng R; Ding J Effects of aspect ratios of stem cells on lineage commitments with and without induction media. Biomaterials 2013, 34, 930–939. [PubMed: 23140997]

[94]. Salasznyk RM; Klees RF; Williams WA; Boskey A; Plopper GE Focal adhesion kinase signaling pathways regulate the osteogenic differentiation of human mesenchymal stem cells. Exp. Cell. Res 2007, 313, 22–37. [PubMed: 17081517]

[95]. Khatiwala CB; Kim PD; Peyton SR; Putnam AJ ECM compliance regulates osteogenesis by influencing MAPK signaling downstream of RhoA and ROCK. J. Bone Miner. Res 2009, 24, 886–898. [PubMed: 19113908]

[96]. Liu YS; Liu YA; Huang CJ; Yen MH; Tseng CT; Chien S; Lee OK Mechanosensitive TRPM7 mediates shear stress and modulates osteogenic differentiation of mesenchymal stromal cells through Osterix pathway. Sci. Rep, 2015, 5, 16522. [PubMed: 26558702]

[97]. Sen B; Xie Z; Case N; Thompson WR; Uzer G; Styner M; Rubin J mTORC2 regulates mechanically induced cytoskeletal reorganization and lineage selection in marrow- derived mesenchymal stem cells J. Bone Miner. Res, 2014, 29(1), 78–89. [PubMed: 23821483]

[98]. Dahl KN; Ribeiro AJ; Lammerding J Nuclear shape, mechanics, and mechanotransduction. Circ. Res 2008, 102, 1307–1318. [PubMed: 18535268]

[99]. Galindo M; Pratap J; Young DW; Hovhannisyan H; Im HJ; Choi JY; Lian JB; Stein JL; Stein GS; Van Wijnen AJ The bone-specific expression of Runx2 oscillates during the cell cycle to support a G1-related antiproliferative function in osteoblasts. J. Biol. Chem 2005, 280, 20274–20285. [PubMed: 15781466]

[100]. Tang J; Peng R; Ding J The regulation of stem cell differentiation by cell–cell contact on micropatterned material surfaces. Biomaterials 2010, 31, 2470–6. [PubMed: 20022630]

[101]. Valamehr B; Jonas SJ; Polleux J; Qiao R; Guo S; Gschweng EH; Stiles B; Kam K; Luo TM; Witte ON; Liu X; Dunn B; Wu H Hydrophobic surfaces for enhanced differentiation of embryonic stem cell-derived embryoid bodies. Proc. Natl. Acad. Sci. U.S.A 2008, 105, 14459–14464. [PubMed: 18791068]

[102]. Brammer KS; Choi C; Frandsen CJ; Oh S; Jin S Hydrophobic nanopillars initiate mesenchymal stem cell aggregation and osteo-differentiation. Acta Biomater 2011, 7, 683–690. [PubMed: 20863916]

[103]. Ivarsson M; McWhirter A; Borg TK; Rubin K Type I collagen synthesis in cultured human fibroblasts: regulation by cell spreading, platelet-derived growth factor and interactions with collagen fibers. Matrix Biology 1998, 16, 409–425. [PubMed: 9524361]

[104]. Klein MO; Bijelic A; Toyoshima T; Götz H; Von Koppenfels RL; Al- Nawas B; Duschner H Long- term response of osteogenic cells on micron and submicron- scale- structured hydrophilic titanium surfaces: sequence of cell proliferation and cell differentiation. Clin. Oral Implants Res 2010, 21, 642–649. [PubMed: 20666791]

[105]. Donos N; Hamlet S; Lang NP; Salvi GE; Huynh- Ba G; Bosshardt DD; Ivanovski S Gene expression profile of osseointegration of a hydrophilic compared with a hydrophobic microrough implant surface. Clin. Oral Implants Res, 2011, 22(4), 365–372. [PubMed: 21561478]

[106]. Paduano F; Marrelli M; Alom N; Amer M; White LJ; Shakesheff KM; Tatullo M Decellularized bone extracellular matrix and human dental pulp stem cells as a construct for bone regeneration. J. Biomater. Sci. Polym. Ed, 2017, 28(8), 730–748. [PubMed: 28285576]

[107]. Golub EE, Boesze-Battaglia K The role of alkaline phosphatase in mineralization. Curr. Opin. Orthop, 2007, 18(5), 444–448.

[108]. Engler AJ; Sen S; Sweeney HL; & Discher DE Matrix elasticity directs stem cell lineage specification. Cell, 2006, 126(4), 677–689. [PubMed: 16923388]

[109]. Wen JH; Vincent LG; Fuhrmann A; Choi YS; Hribar KC; Taylor-Weiner H; Engler AJ Interplay of matrix stiffness and protein tethering in stem cell differentiation. Nat. Mater, 2014, 13(10), 979. [PubMed: 25108614]

[110]. Kilic C; Girotti A; Rodriguez-Cabello JC; Hasirci V A collagen-based corneal stroma substitute with micro-designed architecture. Biomater. Sci, 2014, 2(3), 318–329. [PubMed: 26827754]

Highlights

- Micropillars increased cell attachment but reduced proliferation rate at early time points.
- Oxygen plasma treatment enhanced both cell attachment and proliferation rate on all substrates.
- Untreated hydrophobic arrays induced osteogenic differentiation of DPSCs without chemical induction over 28 days of culture.
- The expression levels of osteogenic genes were positively correlated with the degree of nuclear deformations.

A

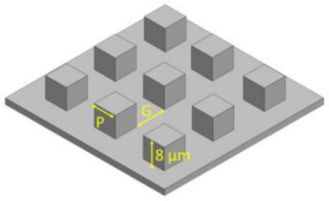

Surface	Pillar Side Length (P) (μm)	Interpillar Gap Length (G) (μm)	Pillar Height (μm)
P4G4	4	4	8
P8G8	8	8	8
P16G16	16	16	8

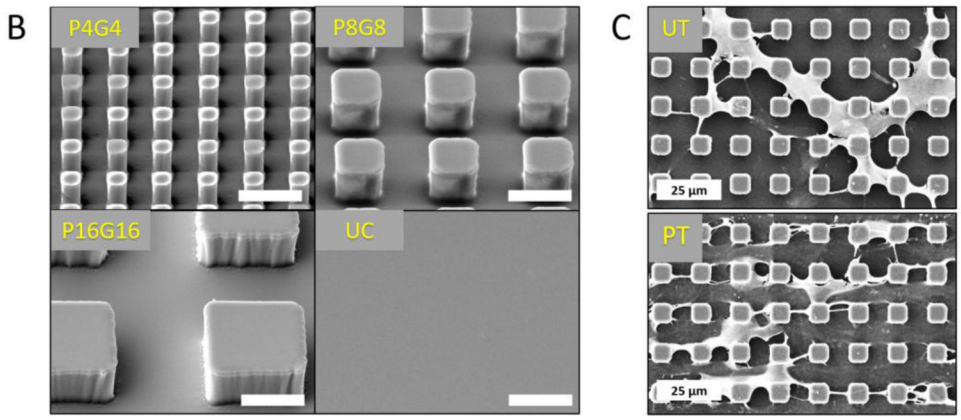

Figure 1.

Design and surface modification of PMMA films. (A) Designed dimensions of three PMMA surfaces decorated with square prism micropillars. (B) SEM micrographs of the micropatterned PMMA films. Scale bars: 10 μm. (C) Representative SEM micrographs of DPSCs on untreated (UT) and plasma treated (PT) P8G8 surfaces on Day 7.

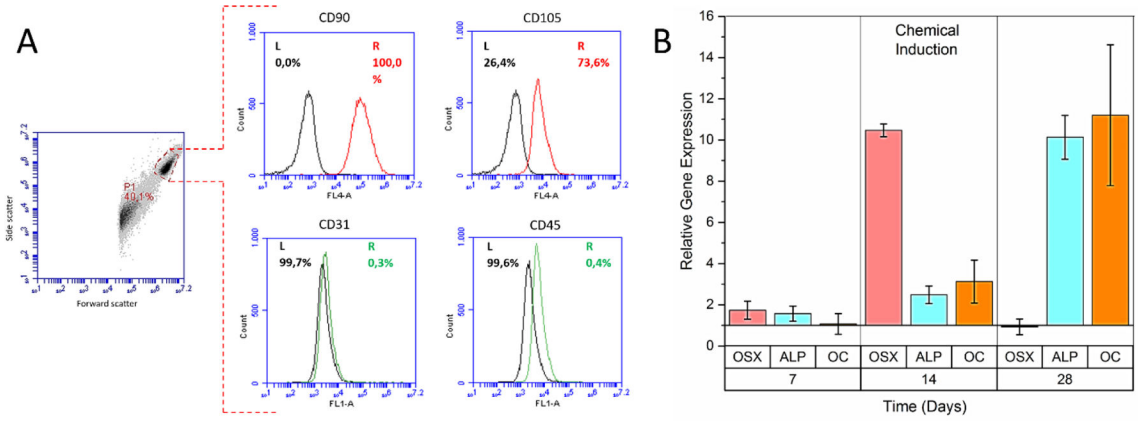

Figure 2.

Characterization of the cells isolated from dental pulp tissues. (A) Flow cytometry histograms of passage 2 cells gated on the forward and side scatter of analyzed particles for the expression of MSC positive CD90 and CD105 (red), and negative CD31 and CD45 (green) surface markers. Black curves: Unstained control. (B) Relative expression of the osteogenic marker genes osterix (OSX), alkaline phosphatase (ALP), and osteocalcin (OC) by the cells chemically induced with dexamethasone. Expression levels in the chemical induction group were normalized to the corresponding levels in the maintenance media without osteogenic supplements.

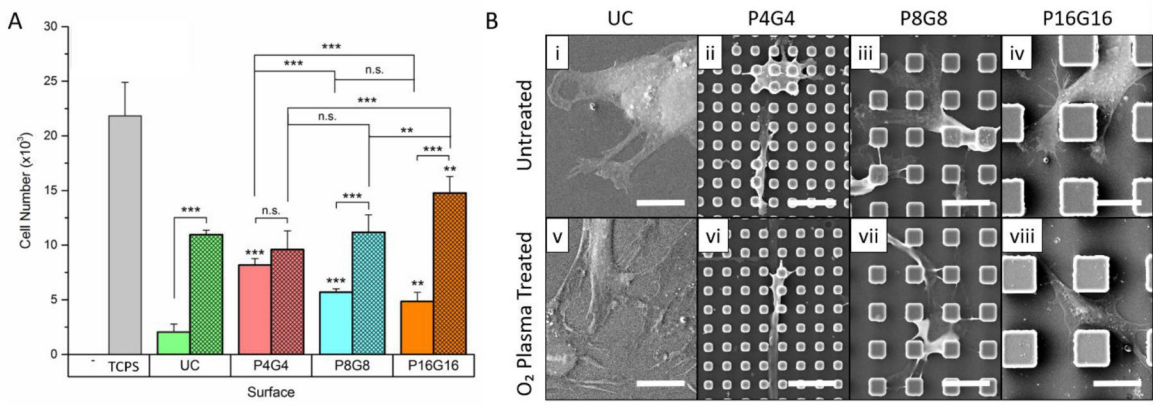

Figure 3.

Cell attachment on the substrates. (A) The number of DPSC on PMMA films 16 h after cell seeding. (Seeding density: 3×10^4 cells.cm^{-2}). Hatched columns represent oxygen plasma treated substrates. Data represent mean ± SD of three replicates, *p < 0.05, **p < 0.01 and ***p < 0.001. Asterisks above the bars represent significance compared to the unpatterned control. n.s.: not significant. (B) SEM micrographs of DPSCs on (i-iv) untreated and (v-viii) oxygen plasma treated substrates on Day 1 (Scale bars: 20 μm, UC: unpatterned control).

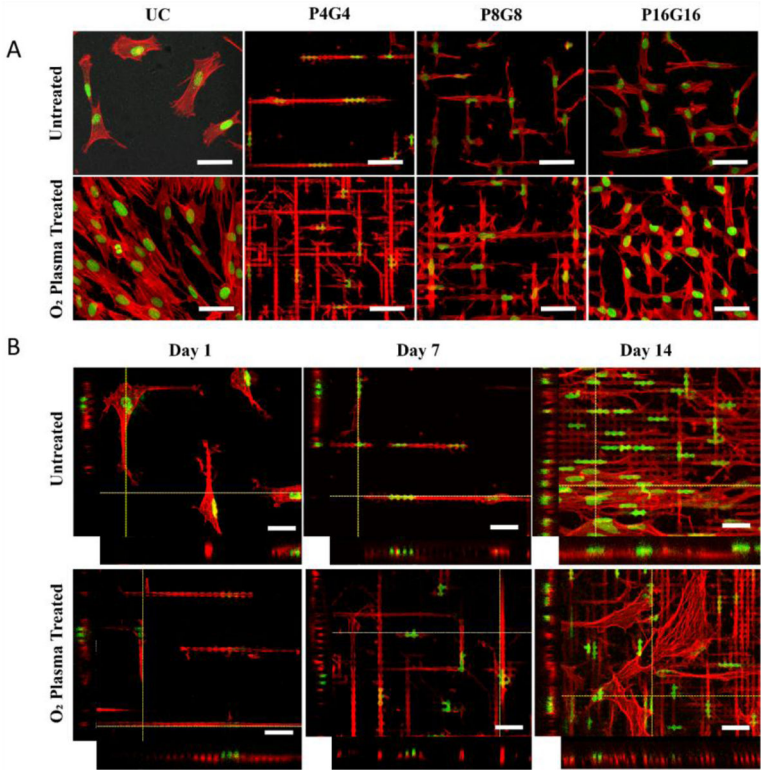

Figure 4.

Nuclear and cytoskeletal morphology of DPSCs on the substrates. (A) Confocal micrographs of the DPSCs on PMMA films on Day 7 (Scale bars: 50 μm). (B) Z-stack images of the cells on P4G4 surface on Days 1, 7 and 14 (Scale bars: 30 μm). Red: Actin cytoskeleton (Alexa Fluor 488-conjugated Phalloidin), green: nucleus (DRAQ5).

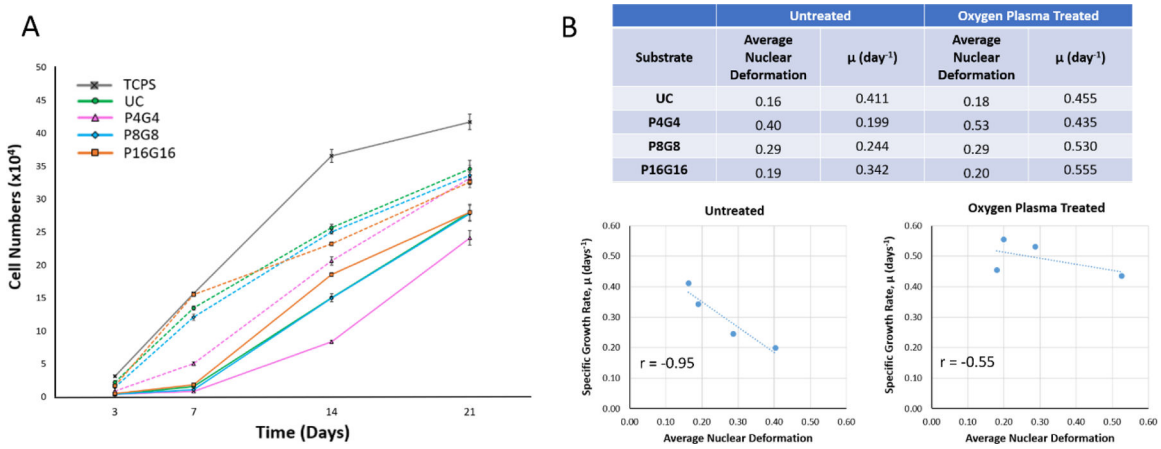

	Untreated		Oxygen Plasma Treated	
Substrate	Average Nuclear Deformation	μ (day⁻¹)	Average Nuclear Deformation	μ (day⁻¹)
UC	0.16	0.411	0.18	0.455
P4G4	0.40	0.199	0.53	0.435
P8G8	0.29	0.244	0.29	0.530
P16G16	0.19	0.342	0.20	0.555

Figure 5.

Proliferation of DPSCs on PMMA substrates. (A) Cell numbers on the substrates determined by Alamar blue assay on days 3, 7, 14, and 21 (Seeding density: 10^4 cells.cm^{-2}). Dashed lines represent proliferation on the oxygen plasma treated substrates. (B) Analysis of correlation between average nuclear deformations and specific growth rates (μ, day^{-1}) on untreated and oxygen plasma treated substrates between Days 3 and 7.

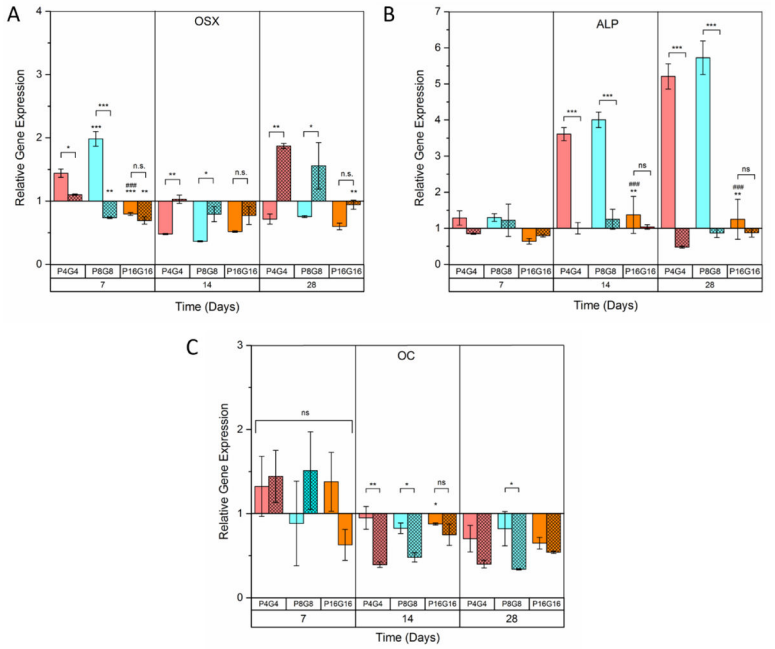

Figure 6.

Relative expression of the osteogenic marker genes (A) Osterix (OSX), (B) Alkaline phosphatase (ALP), and (C) Osteocalcin (OC) The gene expressions on micropillar decorated films were normalized to the mean values on the unpatterned control films. Hatched columns represent oxygen plasma treated substrates. Data represents mean ± SD for four samples, *$p < 0.05$, **$p < 0.01$ and ***$p < 0.001$. *, # and + above the bars represent significance compared to smooth, P4G4 and P8G8 surfaces, respectively. n.s: not significant.

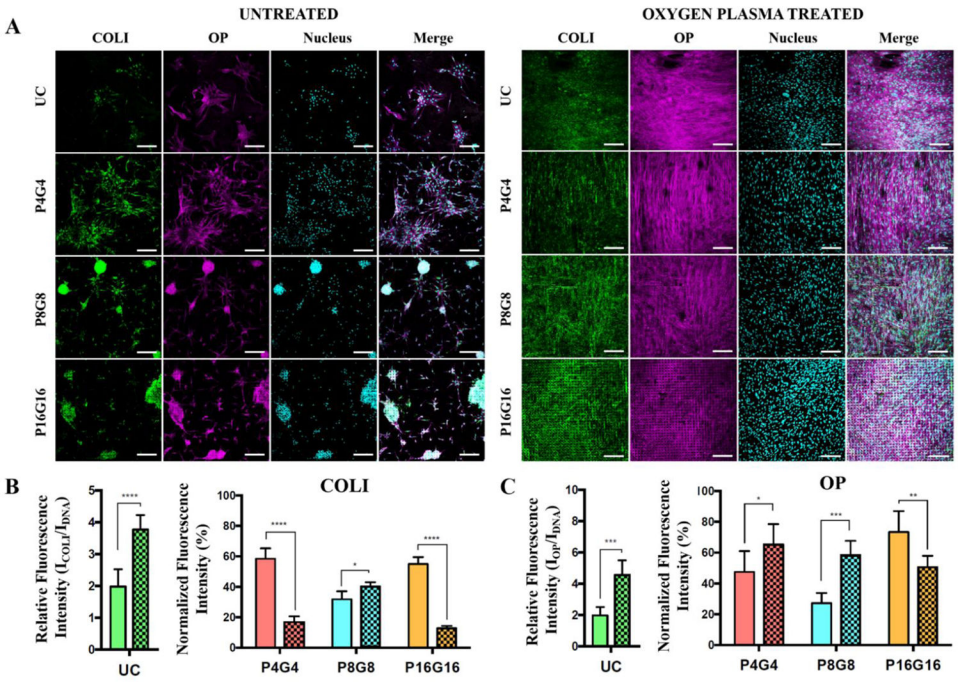

Figure 7.

Bone matrix deposition by DPSCs on PMMA films. (A) Immunohistochemical staining of collagen type I (COLI) and osteopontin (OP) on Day 28. Green: COLI, purple: OP, cyan: nucleus (DRAQ5). Scale bars: 200 μm. Semiquantitative analysis of the relative fluorescence intensities of (A) COLI and (B) OP on the substrates normalized to DNA signal. Relative intensities on patterned surfaces were normalized to unpatterned controls. Hatched columns represent oxygen plasma treated surfaces. Data represents mean ± SD, *$p < 0.05$, **$p < 0.01$, ***$p < 0.001$, and ****$p<0.0001$.

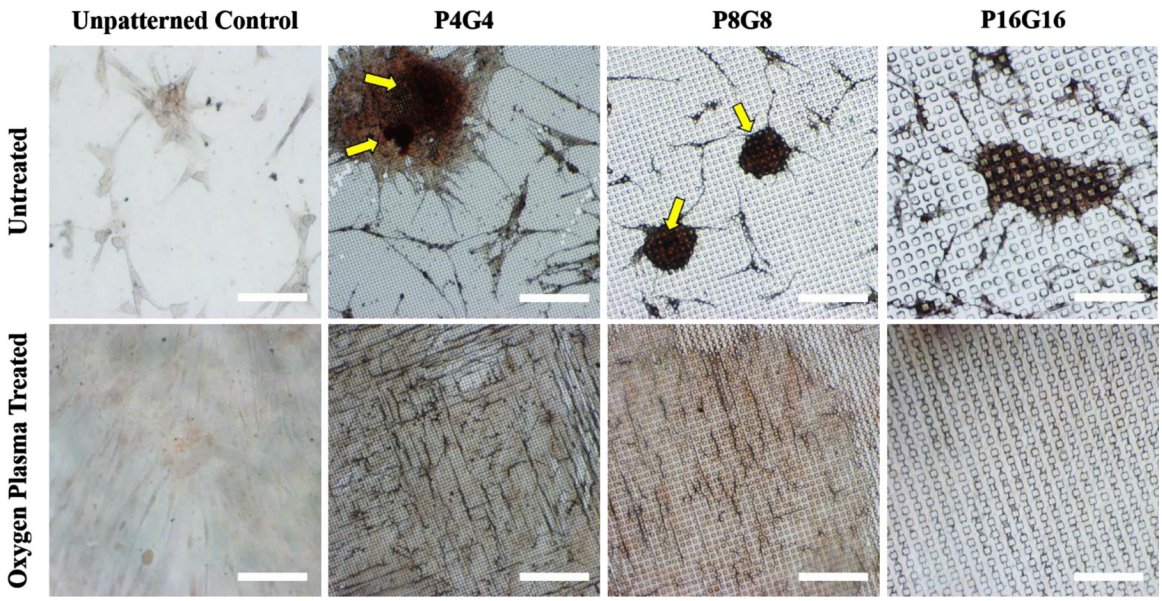

Figure 8.

Alizarin red staining of DPSCs on PMMA films on Day 28. Yellow arrows point dark red accumulations depicting calcific deposition by the cells. Scale bars: 200 μm.